Magnetic field effects on intersubband transitions in quantum cascade structures

Vadim M. Apalkov[a], Anjana Bagga[b], Tapash Chakraborty[b]

[a]Department of Physics and Astronomy, Georgia State University, Atlanta, Georgia 30303, USA

[b]Department of Physics and Astronomy, University of Manitoba, Winnipeg, Canada R3T 2N2

ABSTRACT

We report on our study of the effects of external magnetic field on the intersubband optical transitions in quantum cascade systems. We address the properties of two types of cascade structures: terahertz quantum cascade lasers and quantum dot infrared photodetectors. In both cases we study the optical properties of active regions of the systems: optical emission in the case of quantum cascade lasers and optical absorption in the case of photodetectors. The new features and new peaks in the optical spectra appear in the tilted magnetic field for quantum cascade lasers and in the parallel magnetic field for quantum dot photodetectors. In the relation to the possible spintronic application of cascade structures we study interplay of spin-orbit and magnetic field effects in cascade systems. If spin-orbit coupling is strong enough then at finite parallel magnetic field the optical emission spectra of quantum cascade lasers have two-peak structure.

Keywords: quantum cascade lasers, nanostructures, infrared photodetectors, magnetic field

1. INTRODUCTION

Quantum cascade structures (QCS) consist of specially designed superlattices of quantum wells, quantum dots, or their combinations. Optical transitions between the subband levels of dimensional quantization in the growth direction of the QCS occur within the active region. In these subbands, motion of electrons in the growth direction is frozen and electron motion is, to a good approximation, two-dimensional in the quantum wells and zero dimensional in the quantum dots. The examples of quantum cascade structures are quantum cascade lasers[1] and quantum well[2] or quantum dot[3] infrared photodetectors.

In the case of quantum cascade lasers (QCL) the active region consists of few specially designed quantum wells. In the initial state the electrons are in the excited subbands and the optical transitions resulting in photon emission occur between the excited and the ground subbands of active region. In the photodetectors the electrons initially are in the ground state of the active region. The optical transitions with absorption of photons are between the ground and excited states of active region.

The optical transitions in quantum cascade systems occur between the discrete subbands or discrete levels of dimensional quantization, resulting in emission or absorption of light at discrete frequencies. In this relation it becomes very important to tune the optical frequency for a given configuration of cascade system. One of the ways to tune the optical properties of QCS is to apply an electric field, i.e. bias voltage, along the growth direction of QCS. In this approach the bias voltage will not only shift the relative positions of energy levels in active region of QCS and correspondingly the response frequency, but also modify the current through the system. Here we consider another approach to the problem of tuning of optical properties of QCS. This approach is based on application of magnetic field to quantum cascade structures. The effect of magnetic field on the optical and transport properties of quantum well structures has been studied extensively for different systems.[4,5] The main effect of parallel magnetic field is the momentum shift of the electron dispersion. This fact can strongly influence the processes, such as tunneling and optical transitions, where conservation of two-dimensional momentum is involved. In optics this results, for example, in the shift of quantum cascade laser lines and its broadening,[6] although the disorder can suppress the effect of magnetic field.[7]

In the present paper we study the effects of magnetic field on the optical transitions for specially designed systems of quantum wells and quantum dots, which are the building blocks of quantum cascade lasers and

Nanomodeling II, edited by Akhlesh Lakhtakia, Sergey A. Maksimenko,
Proc. of SPIE Vol. 6328, 632802, (2006) · 0277-786X/06/$15 · doi: 10.1117/12.679790

quantum dot infrared photodetectors. We restrict the systems only by their active region and do not address the question of how magnetic field affects the rates of escape of electrons from active region and trapping of electrons into the active region. In the case of photodetectors the escape process usually has the tunneling nature, i.e. under applied bias voltage the electron tunnels through the potential barrier into the continuous states and contribute to the photocurrent. The parallel magnetic field introduces additional potential barrier, which should suppress the tunneling and correspondingly the escape rate.[8] For some parameters of photodetectors the main channel of escape tunneling is the phonon assisted tunneling. In this case the emission of the phonons suppresses the potential barrier due to magnetic field. Then the tunneling rate can have weak dependence on magnetic field.[8]

We analyze the optical properties of QCS in magnetic field for a few typical geometries of active region. The Hamiltonian of the system is written in the effective mass approximation and then the wavefunctions and energy spectra are found numerically for a finite size system. With the known wavefunctions and energy spectra the optical spectra can be easily found. The magnetic field, B, introduces an additional length scale - magnetic length, $l_B = (\hbar c/eB)^{\frac{1}{2}}$. Here e is the absolute value of electric charge. We should expect the new magnetic field related effects when the characteristic size of the system, i.e. the width of the wavefunctions or the spatial separation between different wavefunctions, becomes of the order of magnetic length. In this case we should expect the modification of optical spectra of quantum cascade structures.

The paper is organized as follows. In Sect. 2 we discuss the effects of magnetic field on the optical transitions in terahertz quantum cascade lasers. The specific feature of terahertz cascade lasers is that their active regions have large spatial size. Therefore the energy and optical spectra of active regions become very sensitive to external magnetic field. In Sect. 3 we study the properties of quantum cascade lasers with strong spin-orbit interaction. We show that even with spin-orbit coupling the optical spectra are not modified at zero magnetic field. At finite parallel magnetic field the optical spectra have two-peak structure, which is completely due to spin-orbit interaction. In Sect. 4 we present the analysis of optical spectra of quantum dot infrared photodetectors in parallel magnetic field. The presence of quantum dot in the active region make the system more sensitive to the parallel magnetic field. Concluding remarks are presented in Sect. 5.

2. QUANTUM CASCADE LASERS: TILTED MAGNETIC FIELD

Here we consider the active region of quantum cascade laser (QCL) and study the optical properties in the regime of terahertz (1-10 THz) radiation.[9–12] This regime is very important for development of THz sources with high radiation intensity. The typical energy scale of the energy spectra of the active region of terahertz QCL is about 10-20 meV. Such energy scale can be achieved only in the systems with large size of active region, which is about 50 nm. Due to large size of active region and correspondingly large width of the wavefunctions the observable effects of magnetic field should be expected at small magnetic fields around 1-3 T. This is opposite to the case of high frequency QCL where the characteristic magnetic field[7] of the quantum cascade structure is around 10 T.

Analyzing the behavior of electron in magnetic field we can conclude that there are two major effects related to application of magnetic field to the system of quantum wells. The first one is due to parallel magnetic field. If the field is weak enough than it can be considered as a perturbation and results in the shift of 2D dispersion law in the momentum space. The shift is different in the different subbands of active region. Finally, in the optical spectra this results in the blue shift and broadening of the emission line.[7] This picture is valid until the magnetic length is much larger than the typical width of the structure. Another effect is related to perpendicular magnetic field. The application of perpendicular magnetic field results in Landau quantization of electron motion in 2D plane. During the optical transitions there is conservation of Landau level index. Without taking into account the other non-optical transitions between subbands, i.e. due to optical and acoustic phonons, we can say that perpendicular magnetic field will not modify the emission spectra.

It was shown that application of tilted magnetic field results in new interesting effects.[13] An externally applied magnetic field that is tilted from the direction perpendicular to the electron plane provides two magnetic field components: The parallel component of the field causes a shift in the energy dispersion as described above. The perpendicular component, on the other hand, causes quantization of the subbands. Because of the shifts of the center of the Landau orbit in the momentum space, combined intersubband-cyclotron transitions, in addition

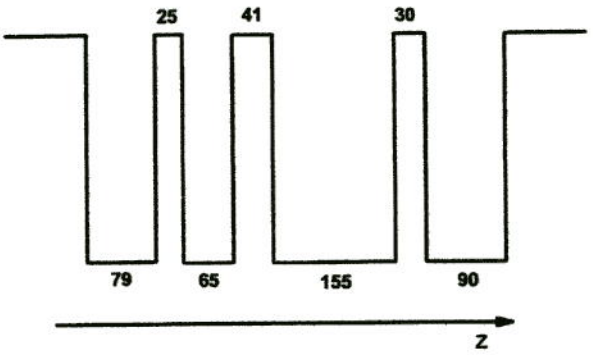

Figure 1. The conduction band of active region of quantum cascade laser is shown schematically for $GaAs/Al_{0.15}Ga_{0.85}As$ structure. The numbers show the width of corresponding regions in Å.

to the usual intersubband transitions, are allowed.[14,15] The detailed calculations[7] indicate that as the subbands quantize into discrete Landau levels, new luminescence peaks in QCL appear that correspond to those new transitions. The peaks exhibit a prominent red shift but can be made as sharp and large as the zero-field case by tuning the applied magnetic field.

The situation in terahertz QCL is more complicated, since the system becomes more sensitive to the external magnetic field. This is due to a larger size of the active region or a smaller energy scale within the active region of QCL. Below we present our analysis of the optical spectra of terahertz QCL.

The typical active region of terahertz QCL[12] is shown schematically in Fig. 1. Due to quantization of electron motion in z-direction there are 5 subbands within active region of QCL. The optical transitions occur between the 5th and 4th subbands, i.e. initially electrons occupy the 5th subband. We describe the system within an effective mass approximation. With the tilted magnetic field the Hamiltonian corresponding to the active region of QCL has the following form

$$\mathcal{H} = \left(\vec{p} + \frac{e}{c}\vec{A}\right) \frac{1}{2m^*(z)} \left(\vec{p} + \frac{e}{c}\vec{A}\right) + V(z), \tag{1}$$

where $V(z)$ is the potential describing the conduction band profile, shown in Fig. 1; m^* is an electron effective mass, which depends on the material, and $\vec{A} = (zB_\parallel, xB_\perp, 0)$ is a vector potential. Here the magnetic field has only y and z components, $\vec{B} = (0, B_\parallel, B_\perp)$. We also characterize magnetic field by the magnetude, B, and tilt angle, θ: $B_\parallel = B\sin(\theta)$, $B_\perp = B\cos(\theta)$. In y direction the system is translational invariant and the states are characterized by y component of the electron momentum. The electron dynamics in x and z directions are coupled. We find the corresponding energy spectra and wavefunctions numerically for a finite-size system. Then the emission spectra is found from the expression

$$I(\omega) = I_0 \sum_{i,k_y}^{\prime} f_{i,k_y} \sum_f \left| \int d\vec{\rho} dz \psi^*_{i,k_y}(\vec{\rho}, z) z \psi_{f,k_y}(\vec{\rho}, z) \right|^2 \delta\left(E_{i,k_y} - E_{f,k_y}\right), \tag{2}$$

where $\vec{\rho} = (x, y)$ is the 2D vector, and the sum over the initial states, i, goes over all occupied states. In Eq. (2) we assumed that electrons in the inital state, i.e. before optical transitions, are in the quasiequalibrium, which is characterized by chemical potential, μ, and the Fermi distribution function f_{i,k_y}. To find the initially occupied states and correspondingly the distribution function f_{i,k_y} in the magnetic field we calculate the projection, p_i, of each state i on the 5th subband of active region, where the states of the 5th subband are calculated at zero perpendicular component of magnetic field. Then we assume that in the initial state of the electron system the possible occupied levels are those with $p_i > 0.5$. Based on this criterion we calculate the chemical potential,

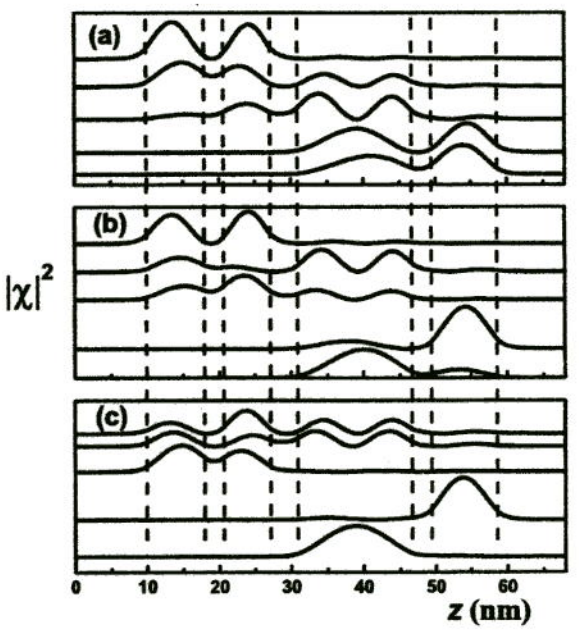

Figure 2. The electron probability density, $|\chi(z)|^2$, is shown for the first 5 subbands of active region of QCL illustrated in Fig. 1 and for different values of parallel magnetic field: (a) $B_{\parallel} = 0$ T; (b) $B_{\parallel} = 1.5$ T; (c) $B_{\parallel} = 3$ T. The perpendicular component of magnetic field is zero. The dashed lines show the positions of quantum wells (see Fig. 1).

μ, corresponding to electron 2D density N_e. In the calculations below we assume that $N_e = 10^{10}\ cm^{-2}$ and temperature is 50 K.

The subband wavefunctions of active region of terahertz QCL is very sensitive to the value of parallel magnetic field. At zero perpendicular magnetic field the wavefunctions can be classified by 2D momentum in the (x, y) plane and can be written as $\chi_i(z)\exp(i\vec{k}\vec{\rho})$, where $\chi_i(z)$ is the ith subband wavefunction, which has strong dependence on parallel magnetic field. This dependence is shown in Fig. 2. We can see that the envelope functions for the first and second subband remain almost the same up to magnetic field 3 T. Only at 3 T (Fig. 2c) we have the mixture between the first and second subbands. At the same time the subbands with the higher energy have very strong dependence on the parallel magnetic field. The mixture between these subbands is strong already at 1.5 T (Fig. 2b). As we mentioned before the origin of such strong dependence is the large size of active region of QCL and correspondingly the large width of subband wavefunctions.

In Fig. 3 we present the results of calculation of optical emission spectra. The most pronounced magnetic field effects are at field 3 T. At lower magnetic fields we can see the small structure due to Landau quantization of 2D motion induced by perpendicular component of magnetic field. In Fig. 3a the results are shown for $B = 2$ T and different tilt angle. With increasing tilt angle we can see the formation of the second peak in the emission spectra, corresponding to optical transitions between different Landau levels of different subbands. The separation between the peaks is small due to small values of magnetic field and finally the second peak disappers at large tilt angle. At higher magnetic field, $B = 3$ T (Fig. 3b), the tendency remains the same but the peaks become more pronounced. At intermediate tilt angle the peaks can be resolved and clear two-peak structure can be observed. At larger tilt angle there is a single strong peak and many small peaks in emission spectra. Finally, at $\theta = 90^0$, i.e. at parallel magnetic field, we should expect a single peak.

In Fig. 3c we present the different way to apply the tilted magnetic field. In this case we fix the parallel component of magnetic field equal to $B_{\parallel} = 3$ T and change the perpendicular component of magnetic field. Therefore, with increasing $B_{\perp}$ we increase both the tilt angle and the magnitude of magnetic field. Similar to

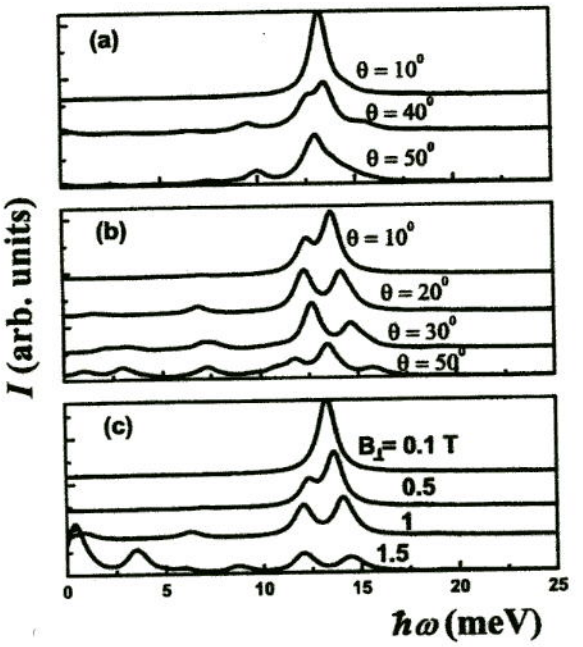

Figure 3. Emission spectra of active region of QCL is shown at tilted magnetic field. (a) the magnetude of magnetic field is $B = 2$ T, the numbers by the lines are tilt angles; (b) the magnetude of magnetic field is $B = 3$ T, the numbers by the lines are tilt angles; (c) the parallel magnetic field is $B_{\parallel} = 3$ T, the numbers by the lines are the values of perpendicular magnetic field, $B_{\perp}$.

Fig. 3b the two-peak structure is clearly seen.

Summarizing the above analysis we can conclude that application of tilted magnetic field to the terahertz QCL results in formation of many peak structure. Usually only two peaks can be resolved with the typical separation between the peaks around 5 meV. Due to large size of the active region of terahertz QCL the magnetic field at which new peaks can be observed is rather small and around 3 T.

3. QUANTUM CASCADE LASERS: SPIN-ORBIT INTERACTION

As it was mentioned above, application of parallel magnetic field to QCL results only in the shift and some broadening of emission line. No additional structure in the emission line should emerge. Here we show that this statement is not exactly true. Additional peak in emission line can be observed in QCL system if there is a strong spin-orbit (SO) interaction in the active region of QCL. In this case the two-peak structure exists in the parallel magnetic field, while at zero magnetic field there is still a single peak. Therefore, the two-peak structure in the emission line can be observed if the parallel magnetic field is applied to the quantum cascade system with strong SO coupling.[16] Below we assume that SO coupling in the active region of QCL is due to *asymmetry* of confinement potential.[17] Many novel effects that are entirely due to the SO interaction have been proposed and some are observed experimentally.[18–21]

The physical origin of SO-induced two-peak structure in the emission spectra is the following. The electron states within each subband of active region of QCL are characterized by a two-dimensional momentum, $\hbar\vec{k}$. The optical transitions between subbands are allowed only between the states with the same momentum $\vec{k}$ and the same spin projection. Since the SO interaction couples the orbital motion and spin, one would expect that the SO coupling should produce two types of optical lines, corresponding to transitions between the same spin orientation of the two subbands and between the different spin orientations. However, for a weak enough disorder only one type of transition is allowed. This is because, for the SO interaction $\alpha(\vec{k} \times \vec{\sigma})\vec{n}$, where α is the

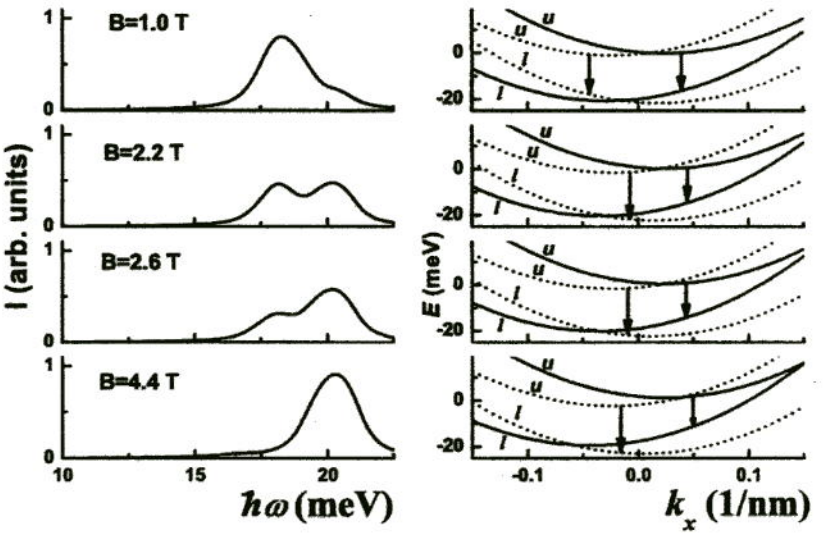

Figure 4. Emission spectra for different values of the parallel magnetic field and for $\alpha_u = -\alpha_l = 45$ meV·nm (left panel) and the corresponding energy spectra of upper and lower subbands as a function of k_x for $k_y = 0$ (right panel). States with a positive value of y projection of spin are shown by solid lines, and with a negative value are shown by dotted lines. The arrows illustrate two types of transitions which results in two-peak structure of emission spectra. The letters "u" and "l" next to the lines stand for upper and lower subbands, respectively.

SO coupling constant, $\vec{\sigma}$ is the spin operator, and $\vec{n}$ is the unit vector normal to the two-dimensional plane,[17] the spin direction is correlated with the direction of momentum, and the spin states will be characterized by definite values of the chirality, i.e. the spin projection on the direction perpendicular to $\vec{k}$. For a weak disorder the optical transitions are allowed only between the states with the same $\vec{k}$. Then the requirement of spin conservation during optical transitions allows only transitions between the states with the same chirality, i.e. only a single optical line should be observed. To observe the two optical lines we need to modify the energy spectra of electrons in different subbands. One way of doing this is by applying a parallel magnetic field. To understand the basic factors which determine the shape of emission line we consider below only two subbands in the active region of the QCL and disregard the effect of parallel magnetic field on the electron dynamics in z direction. Electrons in these subbands will have different positions in the growth direction of the QCL. In other words we assume that $z_u = \langle z \rangle$ (the average value of z for the upper subband) is different from $z_l = \langle z \rangle$ (that of the lower subband). The values of z_u and z_l depends on the structure of the QCL and on the applied voltage. We will consider these quantities as parameters. The wavefunctions of electrons in the upper and lower subbands will then have the form $\Psi_u(x,y,z) = \psi_u(x,y)\chi_u(z)$ and $\Psi_l(x,y,z) = \psi_l(x,y)\chi_l(z)$. The emission spectra of the QCL is determined by the optical transitions between the upper and lower subbands. The intensity I of these transitions is proportional to $|\langle\chi_u|z|\chi_l\rangle\langle\psi_u|\psi_l\rangle|^2$. Since the SO coupling should manifest itself in the (x,y)-planar dynamics we shall study below only the (x,y) part of this expression. To get a large SO coupling the quantum wells in the active region of QCL should be asymmetric. For such a structure the observed values of the SO coupling constant lie in the range of 5 - 45 meV·nm.[20,21]

In the Hamiltonian (1) we keep only the terms which characterize the dynamics of electrons in $x-y$ plane. Then with SO coupling and parallel magnetic field the electron dynamics in the sth subband is described by the following Hamiltonian

$$\mathcal{H}_s = \frac{1}{2m^*}\left(\vec{p}+\frac{e}{c}\vec{A}\right)^2 + \frac{\alpha_s}{\hbar}\left(\left[\vec{p}+\frac{e}{c}\vec{A}\right]\times\vec{\sigma}\right)\vec{n} + \frac{1}{2}g\mu_B B\sigma_y, \tag{3}$$

where the index $s = u, l$ stands for upper and lower subbands respectively, $\vec{\sigma} = (\sigma_x, \sigma_y, \sigma_z)$ is the vector of Pauli spin matrices, α_s is the SO coupling constant for an electron in the s-th subband, m^* is the electron

effective mass, which we assume is the same in both subbands, and the magnetic field is applied in $\hat{y}$ direction. In Eq. (3) we have made an important assumption that the SO coupling is different in different subbands. Only in this case we could get the well-resolved two-peak structure of the optical spectra. Different values of α in different subbands correspond to diagonal transitions in active region of QCL, i.e. the electrons in upper and lower subbands are localized in different quantum wells. As a next step we introduce the gauge $\vec{A} = (Bz, 0, 0)$ and replace z by its average value z_s for the s-th subband. Then the eigenfunctions of the Hamiltonian [Eq. (3)] are classified according to the chirality, $\kappa = \pm 1$, and form two branches of the spectrum

$$E_{s,\kappa}(\vec{k}) = \frac{\hbar^2}{2m^*}\left[k_y^2 + \left(k_x + \frac{z_s}{l_B^2}\right)^2\right] + \kappa\alpha_s\sqrt{\left(k_x + \frac{z_s}{l_B^2} + \frac{1}{2}\frac{g\mu_B B}{\alpha_s}\right)^2 + k_y^2}, \tag{4}$$

The corresponding eigenfunctions are

$$\psi_{s,\kappa}(\vec{k}) = \frac{1}{\sqrt{2}}\begin{pmatrix} 1 \\ -i\kappa\exp\left(i\phi_{s,\vec{k}}\right)\end{pmatrix} e^{ik_x x + ik_y y}, \tag{5}$$

where the angle $\phi_{s,k}$ is related to $\vec{k}$ as

$$\tan\phi_{s,\vec{k}} = \frac{k_y}{k_x + z_s/l_B^2 + \frac{1}{2}g\mu_B B/\alpha_s}. \tag{6}$$

Taking into account the spin conservation during the optical transitions we can write the emission spectra as

$$\begin{aligned} I(\omega) &= I_0\int\frac{d\vec{k}}{(2\pi)^2}\sum_{\kappa_1\kappa_2} f\left[E_{u,\kappa_1}(\vec{k})\right]\left[\psi^\dagger_{u,\kappa_1}(\vec{k})\psi_{d,\kappa_2}(\vec{k})\right]\delta\left(E_{u,\kappa_1}(\vec{k}) - E_{l,\kappa_2}(\vec{k}) - \hbar\omega\right) \\ &= I_0\int\frac{d\vec{k}}{(2\pi)^2}\sum_{\kappa_1\kappa_2} f\left[E_{u,\kappa_1}(\vec{k})\right]\left|1 + \kappa_1\kappa_2 e^{i\left(\phi_{u,\vec{k}} - \phi_{l,\vec{k}}\right)}\right|^2\delta\left(E_{u,\kappa_1}(\vec{k}) - E_{l,\kappa_2}(\vec{k}) - \hbar\omega\right), \end{aligned} \tag{7}$$

where $f(\epsilon) = 1/[\exp(\epsilon - \mu_F)/k_BT + 1]$ is the Fermi distribution function for electrons in the upper subband with the chemical potential μ_F, which corresponds to electron density N_e and temperature T.

It is easy to see that at both zero and large magnetic fields the optical transitions are allowed only for $\kappa_1 = \kappa_2$, i.e. between the states with the same chirality κ. Transitions between different spin branches are allowed only at intermediate values of magnetic field. The existance of different types of optical transitions results in two peak structure of emission line. Below we show that the maximum separation between the peaks will occur when the SO coupling constants α_s have different signs in the upper and lower subbands.

To analyze the possibility to observe SO-induced two-peak structure of the emission spectra of a QCL we have calculated the optical spectra from Eq. (7) for the density of electrons on the upper subband $N_e = 10^{10}$ cm^{-2}. To have the largest SO coupling constant, $\alpha \approx 45$ meV·nm, we assume that the QCL is based on the narrow gap semiconductor,[21] i.e. InAs ($m^*/m = 0.042$ and $g = -14$). We have also fixed the difference $|z_u - z_l|$ at 3 nm and study the optical spectra as a function of the magnetic field. For illustration purpose we introduce the finite energy difference between the energy levels (upper and lower subbands) of the size quantization in the z direction to be 20 meV. This means that without the SO coupling and without a parallel magnetic field the emission spectra consists of a single line centered at 20 meV.

In Fig. 4 the emission spectra are shown for $\alpha_u = -\alpha_l = 45$ meV·nm and for different values of the parallel magnetic field. In the right panel the energy spectra of the upper and lower subbands are shown as a function of k_x for $k_y = 0$. For $k_y = 0$ the electron subbands can be classified by the definite value of y-projection of the spin, σ_y. The solid lines correspond to the positive value of spin, while the dotted lines correspond to the negative values. Transitions resulting in the two-peak emission spectra are shown by arrows in Fig. 4. At small values of the magnetic field these peaks almost coincide and emission spectra has a single peak with a small shoulder. Eventually, with increasing B two peaks can be resolved and at $B \approx 2.2T$ they have the same intensity. At a

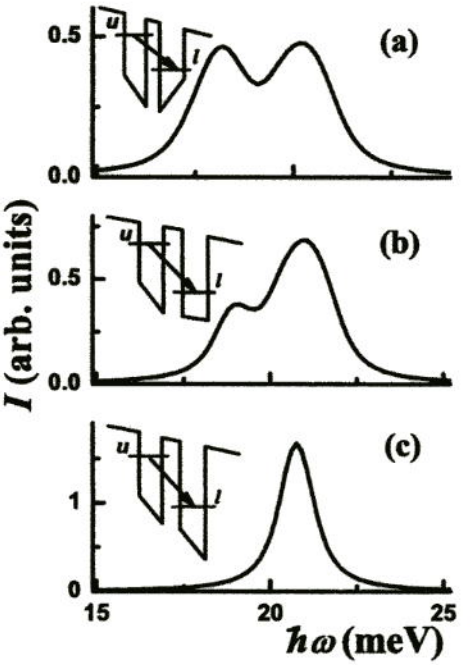

Figure 5. Emission spectra for different structure of active region of QCL, which result in different values of SO coupling in upper and lower subbands: (a) $\alpha_l = -\alpha_u = 45$ meV·nm, (b) $\alpha_u = 0$ and $\alpha_l = 45$ meV·nm, (c) $\alpha_l = \alpha_u = 45$ meV·nm. The schematic illustration of corresponding active regions are shown as an inset.

larger B the intensity of one of the peak will be suppressed and the optical spectrum again acquires a single-peak structure.

The condition $\alpha_u = -\alpha_l$ results in the largest difference between α_u and α_l, i.e. $\alpha_u - \alpha_l = 2\alpha_u$, and the strongest separation between two peaks in the optical spectra. For smaller difference between α_u and α_l the two-peak structure becomes less pronounced and finally it will disappear at $\alpha_u = \alpha_l$. The evolution of the two-peak emission spectra with decreasing difference between α_u and α_l is shown in Fig. 5. For $\alpha_u = 0$ and $\alpha_l = 45$ meV·nm the strongest effect that we can get at some value of the magnetic field is the shoulder in the emission spectra [Fig. 5(b)]. For $\alpha_u = \alpha_l$, and for all values of the magnetic field there is only a single peak [Fig. 5(c)]. While in this case there are also two types of transitions, the width of the corresponding peaks are larger then the separation between them. The inset in Fig. 5 illustrates schematically the structure of two wells which gives the corresponding relation between the SO coupling, where the upper and lower states are localized in different wells.

To summarize, we have shown that in order to observe the two-peak structure, the quantum wells constituting the active region of a QCL should be asymmetric and optical transitions should be diagonal. The next important condition is that the SO couplings in different quantum wells should be different. In this case a two-peak emission line can develop within a certain interval of the parallel magnetic field. This interval is determined by interplay of Zeeman and SO terms in Hamiltonian 3, where Zeeman term is always suppresses two-peak structure.

4. QUANTUM DOT PHOTODETECTORS: PARALLEL MAGNETIC FIELD

In the infrared photodetectors the main optical process is the light absorption, so in the initial state the electron system is in the ground state of the active region. There are different types of infrared photodetectors: quantum well infrared photodetectors,[2] quantum dot photodetectors,[3] and dot-in-a well photodetectors.[22,23] The difference between them is in the structure of active region. To cover different types of optical transitions in infrared photodetectors we will study the dot-in-a well photodetectors.[22] In this type of photodetectors the active region

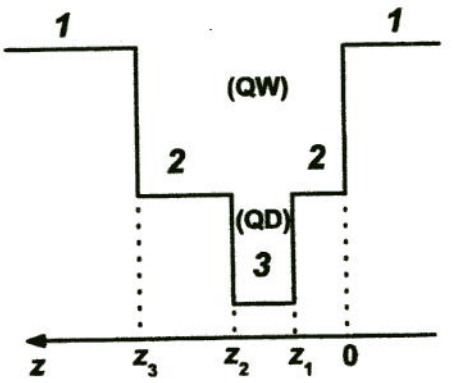

Figure 6. Infrared photodetector with dot-in-well geometry is shown schematically. The structure is shown along the growth direction. The numbers "1", "2", and "3" stand for $GaAs$, $In_xGa_{1-x}As$ (quantum well), and $InAs$ (quantum dot), respectively. For concreteness we choose $x = 0.15$.

consists of usually a single quantum well. Within this quantum well 2D array of quantum dots is grown. The structure is shown schematically in Fig. 6. In the ground state without any external illumination each quantum dot is occupied by 1 or 2 electrons. Under an illumination the electrons are excited into higher energy states. The photodetector shows the response to three different wavelength corresponding to three different types of optical transitions. All transitions occur from the ground state of the dot. The different optical transitions are: (i) bound to bound transitions from the ground state into the excited state of the same dot; (ii) transitions from the ground state of the dot to continuous states of quantum well; (iii) and the transitions from the ground state of the dot to the 3D continuous states of the system. Below we study the effect of magnetic field only on the first two types of optical transitions.

To calculate the photoabsorption rate we assume that electric field, i.e. the bias voltage, is zero. Then we find numerically the energy spectra and corresponding wavefunctions of a single active region of photodetector in parallel magnetic and calculate the optical absorption from the ground state of active region. The Hamiltonian of the electron in active region of photodetector, shown in Fig. 6, has the form similar to Eq. (1)

$$\mathcal{H} = \left(\vec{p} + e\vec{A}\right) \frac{1}{2m^*} \left(\vec{p} + e\vec{A}\right) + V(x, y, z), \tag{8}$$

where $\vec{A} = (Bz, 0, 0)$ and magnetic field is applied in the $\hat{y}$ direction. The potential $V(x, y, z)$ in Eq. (8) depends now on all the coordinates, x, y, and z, and describes the quantum dot and quantum well structure (see Fig. 6). We assume below that quantum dots have pyramidal shape with the sides of the base parallel to x and y axis. The size of the dot is characterized by the size of the base D and the height of the dot h. Below we take h equals to half of the size of the base D, $h = D/2$. In growth (z) direction the system is characterized by parameters z_1, $z_2 - z_1$ (region of QD), and $z_3 - z_2$, see Fig. 6. The size $z_2 - z_1$ is equal to the sum of the height of the dot and the width of wetting layer, 1.24 ML. Below we take the typical values for these parameters: $z_1 = 2$ nm and $z_3 - z_2 = 6$ nm. The width of $GaAs$ layers introduce the finite size of the system. For both layers we take 10 nm. The size of the system in (x, y) plane was $D + 30nm$ in both x and y directions. We used periodic boundary conditions in (x, y) plane. As a next step we find numerically wavefunctions, $\psi_i(\vec{r})$, and energy spectrum, E_i, corresponding to Hamiltonian (8) for a finite size system replacing the derivatives by finite differences. The corresponding Hamiltonian matrix is sparse. To diagonalize the matrix we used Arnoldi-Lanczos algorithm.

With the known wavefunctions we find the optical absorption spectra from the following expression

$$I_x(\omega) = I_0 \sum_f \left| \int d\vec{r} \psi_i^*(\vec{r}) x \psi_f(\vec{r}) \right|^2 \delta\left(E_f - E_i - \hbar\omega\right), \tag{9}$$

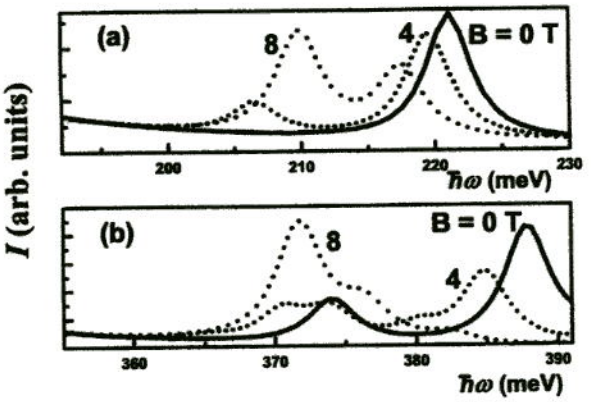

Figure 7. Absorption spectra corresponding to optical transitions from quantum dot to quantum well states are shown for different sizes of quantum dot and different values of parallel magnetic field: (a) $D = 12$ nm; (b) $D = 20$ nm. Numbers by the lines are the magnetudes of magnetic field.

where ψ_i and E_i are the wavefunction and the energy of the initial state, which is the ground state of the system. In Eq. (9) the light is polarized in x direction. This is the one of the main advantage of quantum dot infrared photodetector over the quantum well one. Namely, the quantum well photodetectors can absorb, similar to QCL, only z-polarized light, while the quantum dot photodetectors can absorb both x- and z-polarized photons. Below we assume that the light is x-polarized.

The results of calculations are shown in Figs. 7 and 8. In Fig. 7 we analyze the optical transitions from the bound state of the dot to the continuous states of quantum well. Both for small quantum dots, $D = 12$ nm, and for large quantum dots, $D = 20$ nm, the tendency is the same. At zero magnetic field there is mainly a single peak in the absorption spectra. Application of parallel magnetic field introduces new transitions at low frequency at intermediate magnetic field, $B \sim 5$ T. This results in the two-peak or many-peak structure in the absorption spectra. Finally, at large magnetic field the absorption spectra again have a single peak structure. The peak is red shifted from the zero magnetic field one. The shift is about $10 - 15$ meV. The optical spectra depend on the properties of initial and final states. As we have seen for quantum well structure (see Fig. 2) the ground state has weak dependence on the parallel magnetic field. The reason for weak dependence is the small size of the ground state. In the case of quantum dot-in-a-well detector the ground state has even smaller size because it is localized in the quantum dot. Therefore, for quantum dot photodetectors the ground state can be considered as independent on magnetic field. In this case the transformation of absorption spectra in magnetic field is due to dependence of the final states of the system on the magnetic field.

In Fig. 8 we present the optical transitions within quantum dot states, i.e. transitions from the ground state of quantum dot into excited states of the same dot. For small quantum dots there is only one excited state in the dot. We have found that in this case the effect of magnetic field on optical absorption is very small. For large quantum dots there are many states in the dot. The main transition is to the first excited state. At zero magnetic field transitions to higher excited states are usually strongly suppressed due to optical selection rules and due to different symmetries of excited states of the dot. Application of parallel magnetic field results in the mixture of states with different in-plane symmetry, which increases the intensity of transitions to the excited states of the dot. This behavior is illustrated in Fig. 8(a) for $D = 20$ nm and in-plane polarization of external light. At zero magnetic field there is small peak at ≈ 280 meV. With increasing magnetic field strength we can see the increase of the transition probabilities to other excited states. The positions of these peaks have weak magnetic field dependence, but the heights of the peaks increase with increasing magnetic field.

The properties of the main peak at ≈ 99 meV, which is much stronger than all high frequency peaks, is shown in Fig. 8(b). We can see that the shape of the peak does not depend on the magnetic field. The only effect of magnetic field is very small (~ 1 meV) red shift of the peak at high magnetic field.

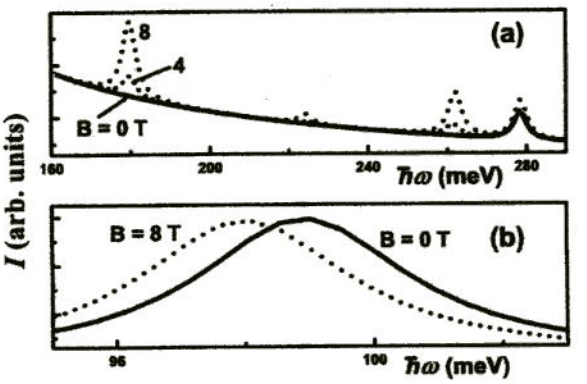

Figure 8. Absorption spectra corresponding to optical transitions within a single quantum dot are shown for different values of magnetic field and in different frequency regions. (a) high-frequency transitions; (b) low frequency peak, corresponding to the main optical transition in the active region of photodetector. Numbers by the lines are the values of magnetic field. The size of quantum dot is $D = 20$ nm.

5. CONCLUSION

Tuning of optical properties of quantum cascade systems can be realized by applying magnetic field to the system. The most interesting effects should be expected in the parallel or in the tilted magnetic fields. In the case of quantum well cascade structures, i.e. the active region consists of specially designed set of quantum wells, the combined intersubband-cyclotron transitions can be seen in the optical spectra in the tilted magnetic field. Such transitions result in the multi-peak structure of emission and absorption optical lines of quantum cascade systems. By changing the tilt angle one can change the positions of peaks and their relative strength. In the parallel magnetic field there is only one peak in the optical spectra, which is broadened and shifted compared to zero field peak. The optical line is red shifted in the case of emission and blue shifted in the case of absorption. The absence of multi-peak structure in the parallel magnetic field is due to translational symmetry of the quantum well cascade system in $x - y$ plane. If within the active region of cascade structure there is strong spin-orbit coupling then even the parallel magnetic field produces two peaks in the optical spectra. This picture describes both the quantum cascade lasers and quantum well infrared photodetectors.

If the system does not have 2D translational symmetry, which is the case of quantum dot infrared photodetector, then the effect of magnetic field on the optical spectra becomes more complicated. Even for parallel magnetic field the absorption line has new features. For the optical transitions within the same quantum dot the optical spectra has multi-peak structure. Each peak corresponds to optical transitions to different bound states of quantum dot. The parallel magnetic field increases the intensity of high frequency transitions but has very weak effect on the relative positions of absorption peaks. For the transitions between bound state of the dot and continuous states of the active region of infrared photodetector the parallel magnetic field shifts the absorption line into low frequency and introduces new absorption peaks in the optical spectrum.

The observable effects of magnetic field on the optical spectra of quantum cascade systems should be expected when the characteristic spatial parameters of active region of the cascade structure becomes of the order of magnetic length.

ACKNOWLEDGMENTS

The work of T.C. has been supported by the Canada Research Chair Program and the Canadian Foundation for Innovation Grant, the work of V.A. has been supported by Petroleum Research Fund under Grant No. 43216-G10.

REFERENCES

1. C. Gmachl, F. Capasso, D.L. Sivco, and A.Y. Cho, Rep. Prog. Phys. **64**, 1533 (2001).
2. B.F. Levine, J. Appl. Phys. **74**, R1 (1993).
3. J. Phillips, K. Kamath, and P. Bhattacharya, Appl. Phys. Lett. **72**, 2020 (1998).
4. B.M. Ashkinadze, E. Linder, E. Cohen, and L.N. Pfeiffer, Phys. Rev. B **71**, 045303 (2005); E. Tutuc, S. Melinte, E. P. De Poortere, M. Shayegan, and R. Winkler, Phys. Rev. B **67**, 241309 (R) (2003); D. Schneider, T. Klaffs, K. Pierz, and F.J. Ahlers, Physica B **298**, 234 (2001); D. Huang and S.K. Lyo, Phys. Rev. B **59**, 7600 (1999); J.P. Eisenstein, T.J. Gramila, L.N. Pfeiffer, and K.W. West, Phys. Rev. B **44**, 6511 (1991).
5. D. Smirnov, C. Becker, O. Drachenko, V. V. Rylkov, H. Page, J. Leotin, and C. Sirtori, Phys. Rev. B **66**, 121305 (2002); J. Alton, S. Barbieri, J. Fowler, H. E. Beere, J. Muscat, E. H. Linfield, D. A. Ritchie, G. Davies, R. Kohler, and A. Tredicucci, Phys. Rev. B **68**, 081303 (2003); G. Scalari, S. Blaser, J. Faist, H. Beere, E. Linfield, D. Ritchie, and G. Davies, Phys. Rev. Lett. **93**, 237403 (2004); V. Tamosiunas, R. Zobl, G. Fasching, J. Ulrich, G. Strasser, K. Unterrainer, R. Colombelli, C. Gmachl, K. West, L. Pfeiffer, and F. Capasso, Semicond. Sci. Technol. **19**, S348 (2004); J. Radovanovic, V. Milanovic, Z. Ikonic, D. Indjin, and P. Harrison, J. Appl. Phys. **97**, 103109 (2005). I. Savic, V. Milanovic, N. Vukmirovic, V. D. Jovanovic, Z. Ikonic, D. Indjin, and P. Harrison, J. Appl. Phys. **98**, 084509 (2005).
6. S. Blaser, L. Diehl, M. Beck, and J. Faist, Physica E **7**, 33 (2000).
7. T. Chakraborty and V.M. Apalkov, Adv. Phys. **52**, 455 (2003).
8. T. Sharpee, M.I. Dykman, and P.M. Platzman, Phys. Rev. B 64, 245309 (2001).
9. R. Kohler, A. Tredicucci, F. Beltram, H.E. Beere, E.H. Linfield, A.G. Davies, D.A. Ritchie, R.C. Iotti, and F. Rossi, Nature **417**, 156 (2002).
10. M. Rochat, L. Ajili, H. Willenberg, J. Faist, H. Beere, G. Davies, E. Linfield, and D. Ritchie, Appl. Phys. Lett. **81**, 1381 (2002).
11. B.S. Williams, H. Callebaut, S. Kumar, Q. Hu, and J.L. Reno, Appl. Phys. Lett. **82**, 1015 (2003).
12. S. Kumar, B.S. Williams, S. Kohen, Q. Hua, and J.L. Reno, Appl. Phys. Lett. **84**, 2494 (2004).
13. V.M. Apalkov and T. Chakraborty, Appl. Phys. Lett. **78**, 1973 (2001).
14. W. Beinvogl and J.F. Koch, Phys. Rev. Lett. **40**, 1736 (1978).
15. T. Ando, Phys. Rev. B **19**, 2106 (1979).
16. V.M. Apalkov, A. Bagga, and T. Chakraborty, Phys. Rev. B **73**, 161304 (2006).
17. Yu. A. Bychkov and E. I. Rashba, Pis'ma Zh. Eksp. Teor. Fiz. **39**, 64 (1984) [JETP Lett. 39, 78 (1984)].
18. D.D. Awschalom, D. Loss, and N. Samarth (Eds.), *Semiconductor Spintronics and Quantum Computation* (Springer, 2002); D. Grundler, Phys. World **15**, 39 (2002); S.A. Wolf, D.D. Awschalom, R.A. Buhrman, J.M. Daughton, S. von Molnar, M.L. Roukes, A.Y. Chtchelkanova, and D.M. Treger, Science **294**, 1488 (2001); G.A. Prinz, Phys. Today **48**, 58 (1995).
19. *Proceedings of the First International Conference on the Physics and Applications of Spin Related Phenomena in Semiconductors*, edited by H. Ohno [Physica E **10** (2001)].
20. T. Chakraborty and P. Pietiläinen, Phys. Rev. Lett. **95**, 136603 (2005); M. Califano, T. Chakraborty and P. Pietiläinen, Phys. Rev. Lett. **94**, 246801 (2005).
21. D. Grundler, Phys. Rev. Lett. **84**, 6074 (2000); C.-M. Hu, J. Nitta, T. Akazaki, H. Takayanagi, J. Osaka, P. Pfeffer, and W. Zawadzki, Phys. Rev. B **60**, 7736 (1999); T. Matsuyama, C.M. Hu, D. Grundler, G. Meier, and U. Merkt, Phys. Rev. B **65**, 155322 (2002); J. Nitta, T. Akazaki, H. Takayanagi, and T. Enoki, Phys. Rev. Lett. **78**, 1335 (1997); G. A. Khodaparast, R.E. Doezema, S.J. Chung, K.J. Goldammer, and M.B. Santos, Phys. Rev. B **70**, 155322 (2004).
22. S. Krishna, S. Raghavan, G. von Winckel, A. Stintz, G. Ariyawansa, S. G. Matsik, and A. G. U. Perera, Appl. Phys. Lett. **83**, 2745 (2003).
23. P. Bhattacharya, X. H. Su, S. Chakrabarti, G. Ariyawansa, and A. G. U. Perera, Appl. Phys. Lett. **86**, 191106 (2005).